International Journal of Nanomedicine

Dovepress
open access to scientific and medical research

Open Access Full Text Article

ORIGINAL RESEARCH

Sono-Immunotherapy Mediated Controllable Composite Nano Fluorescent Probes Reprogram the Immune Microenvironment of Hepatocellular Carcinoma

Yichi Chen[1–3], Bolin Wu[1–3], Haitao Shang[1–3], Yucao Sun[1–3], Huimin Tian[1–3], Huajing Yang[1–3], Chunyue Wang[1–3], Xiaodong Wang[1–3], Wen Cheng[1–3]

[1]Department of Ultrasound, Harbin Medical University Cancer Hospital, Harbin, 150081, People's Republic of China; [2]Department of Interventional Ultrasound, Harbin Medical University Cancer Hospital, Harbin, 150081, People's Republic of China; [3]Institute of Cancer Prevention and Treatment, Heilongjiang Academy of Medical Science, Harbin, 150081, People's Republic of China

Correspondence: Wen Cheng, Department of Ultrasound, Department of Interventional Ultrasound, Harbin Medical University Cancer Hospital, No. 150, Haping Road, Nangang District, Harbin, Heilongjiang Province, 150081, People's Republic of China, Tel +86 13313677182, Fax +86 451 85718392, Email chengwen@hrbmu.edu.cn

Background: Despite the clinical efficacy of immunotherapy in treating malignant tumors, its effectiveness is often hampered by the immunosuppressive nature of the tumor microenvironment (TME). In this study, we propose the design of a nanoscale ultrasound contrast agent capable of triggering macrophage polarization and immunogenic cell death (ICD) for the treatment of hepatocellular carcinoma (HCC) through sonodynamic treatment (SDT) and immunotherapy.

Methods: The re-educator (designated as ICG@C3F8-R848 NBs) is composed of the Toll-like receptor agonist resiquimod (R848) and the sonosensitizer Indocyanine green (ICG), utilizing nanobubbles (NBs) as carriers. The technique known as ultrasound-targeted nanobubble destruction (UTND) employs nanosized microbubbles and low-frequency ultrasound (LFUS) to ensure accurate drug delivery and enhance safety.

Results: Following intravenous delivery, ICG@C3F8-R848 NBs have the potential to selectively target and treat primary tumors using SDT in conjunction with ultrasonography. Importantly, R848 can enhance antitumor immunity by inducing the polarization of macrophages from an M2 to an M1 phenotype.

Conclusion: The SDT-initiated immunotherapy utilizing ICG@C3F8-R848 NBs demonstrates significant tumor suppression effects with minimal risk of systemic toxicity. The utilization of this self-delivery re-education technique would contribute to advancing the development of nanomedicine for the treatment of hepatocellular carcinoma.

Keywords: hepatocellular carcinoma, synergistic sono-immunotherapy strategy, tumor-associated-macrophage

Introduction

Immunotherapy offers significant advantages in the eradication of systemic metastases and tumors.[1,2] Recently, the treatment with immunogenic cell death (ICD) has provided a novel approach to induce systemic anticancer immunity for immunotherapy.[2,3] Among the various therapeutic modalities developed in the ultrasound (US) for noninvasive cancer treatment, sonodynamic treatment (SDT) emerges as a noteworthy and innovative approach. It offers several advantages, including exceptional tissue penetration, non-ionizing properties, precise controllability, and cost-effectiveness.[4,5] As an integral step in the standard SDT procedure, US is utilized to stimulate sonosensitizers, inducing the production of reactive oxygen species (ROS). This ROS generation leads to the death of cancer cells through both the apoptosis and necrosis pathways.[4,6] Based on preclinical animal models, the SDT process has demonstrated the ability to generate tumor antigens that can stimulate the immune system's response against the tumor in the host.[7] Treatment strategies for

Received: 8 July 2023
Accepted: 18 October 2023
Published: 26 October 2023

solid tumors encompass SDT and immunotherapy.[8,9] However, despite the incorporation of therapy-induced ICD in many therapeutic techniques, tumor development can still arise due to immune tolerance mechanisms (ITM).[10–12] Significantly, tumor-associated macrophages (TAMs) play a critical role as the primary immunosuppressive cells within solid tumors. They have the potential to promote tumor cell invasion and migration, and their presence is closely associated with a poor prognosis.[13,14] The M1 and M2 subtypes of TAMs, on the other hand, exhibit opposing immunological functions.[15] In general, M1-like macrophages have the potential to enhance antitumor immunity through the activation of T cells and the phagocytosis of tumor cells. On the contrary, M2-like macrophages exhibit an opposing role by reducing the activity of T cells.[16,17] It is noteworthy that specific stimuli have the ability to alter the phenotype of macrophages, and this flexibility enables an indirect yet effective approach to tumor immunotherapy.[18,19]

Toll-like receptors (TLRs) serve as the primary pattern-recognition receptors in innate immunity.[20–22] Resiquimod and imiquimod have been demonstrated as potent Toll-like receptor (TLR) agonists capable of stimulating immune responses and polarizing M1 macrophages, making them promising candidates for tumor immunotherapy.[23,24] However, the subpar pharmacokinetic characteristics of TLR agonists hinder their ability to meet the requirements for sustaining a prolonged immune response.[25,26] To address this issue, early researchers developed various forms of nanomedicine to enhance the pharmacokinetic characteristics of TLR agonists.[27,28]

In comparison to other nanocarriers, nanobubbles have been extensively utilized as vehicles for a technique called ultrasound-triggered nanodroplet vaporization (UTND).[29] Perfluoro propane (C3F8), as a gas with high relative molecular weight and low solubility, is used as a gas core component and is not easy to overflow from microbubbles. It can effectively maintain the stability of microbubbles and prolong the circulation time of microbubbles in the blood. Therefore, we use C3F8 as the content of nanobubbles (NBs).[30,31] Under ultrasound stimulation, NBs can undergo processes of enlargement, contraction, and eventual destruction. This destruction generates shock waves that enhance cell membrane permeability and facilitate the delivery of intracellular drugs and sonosensitizers. Furthermore, the destruction of NBs raises the local temperature, thereby promoting the production of reactive oxygen species (ROS). Consequently, NBs have emerged as a significant research subject.

In light of the aforementioned factors, a self-delivery macrophage re-educator, named ICG@C3F8-R848 NBs, was developed for SDT-initiated immunotherapy, utilizing sonosensitizers and TLR agonists. Scheme 1 demonstrates that the intermolecular hydrophobic interaction enables the self-assembly of the TLR agonist R848 and the sonosensitizer ICG into uniform nanosized ICG@C3F8-R848 NBs. These nanobubbles can passively accumulate at the tumor site, preventing SDT from promoting the growth of the primary tumor. Furthermore, the SDT performed by ICG@C3F8-R848 NBs has the potential to repolarize M2 macrophages into M1 macrophages, thus rewiring the tumor microenvironment. The combination of SDT and immunotherapy for solid tumor therapy can be mutually reinforced by the presence of self-delivery macrophage re-educators such as ICG@C3F8-R848 NBs. This innovative approach provides valuable insights into the development of translational nanomedicine for tumor treatment, while ensuring good biosafety standards. ICG in ICG@C3F8-R848 NBs effectively generate singlet oxygen under ultrasound irradiation to kill tumors. A large number of cell necrosis leads to the secretion and enrichment of various inflammatory cytokines in the tumor microenvironment after phototherapy, causing the recruitment of TAM and the polarization of the M2-like phenotype, thereby inducing immune escape and recurrence of residual tumor cells. The presence of the small molecule R848 confers excellent properties in reshaping the inflammatory microenvironment and significantly translates M2-like TAMs into M1-like phenotypes. The repolarization of TAMs effectively reshaped the immunosuppressive microenvironment in residual tumors after sonodynamic therapy, thereby saving CTL and reducing the proportion of other immunosuppressive cells such as MDSCs and Tregs.

Material and Methods

Materials

Avanti Polar Lipids (Alabaster, AL) provided the 1.2-Distearoyl-sn-glycerol-3-phosphocholine (DSPC) and 1.2-stearoyl-sn-glycerol-3-phosphoethanolamine-N-(methoxy [polyethylene glycol]-2000) (DSPE-PEG-2000). ICG was supplied with 20.70-Dichlorofluorescin diacetate (DCFH-DA) by Shanghai Yuan Ye Bio-Technology Co., Ltd. in Shanghai, China. The

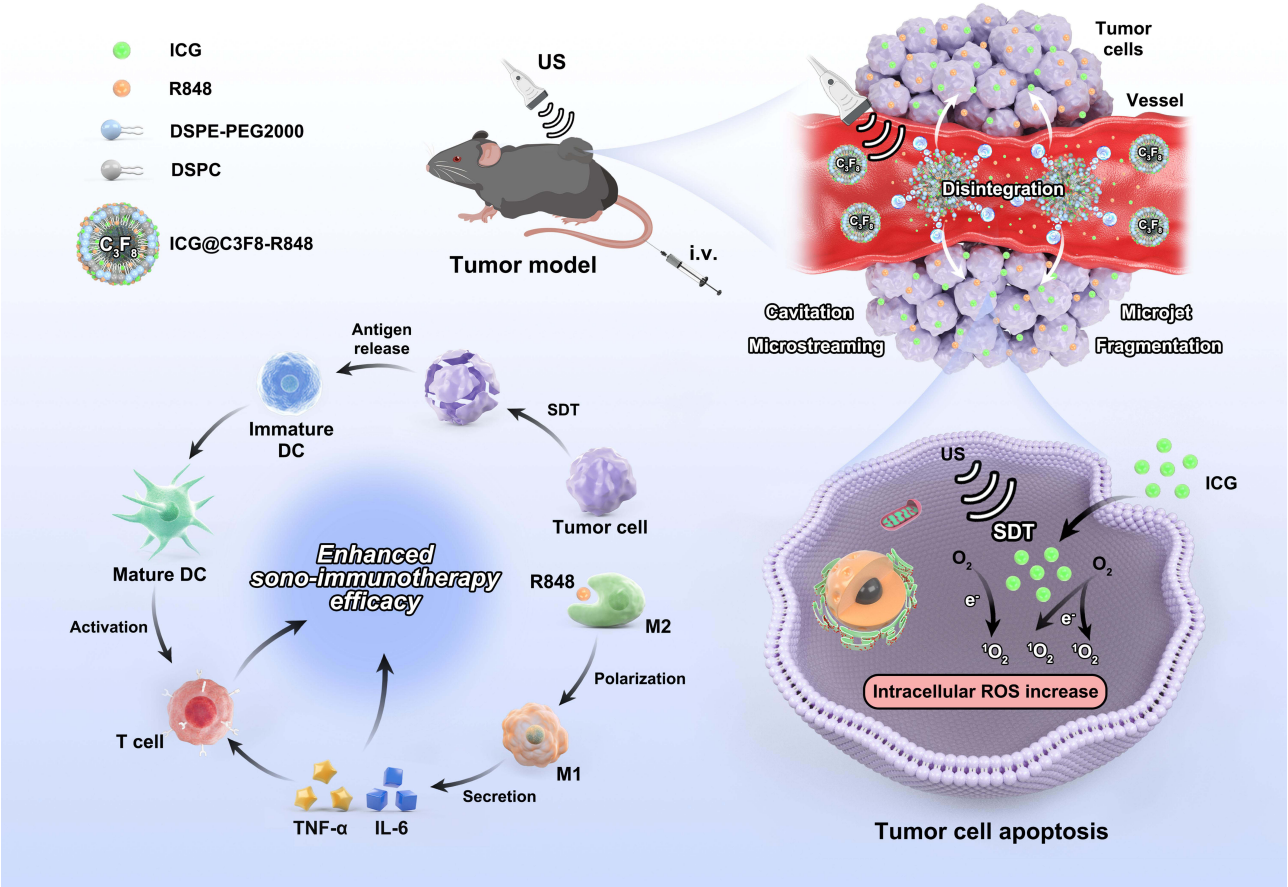

Scheme 1 Schematic illustration of ICG@C3F8-R848 NBs construction, and as an efficient drug with US proposed antitumor strategy.

Cell counter kit-8 (CCK-8) and Annexin V-FITC Apoptosis Detection Kit were purchased from BD Pharmingen. Shanghai MCE Chemicals Technology (Shanghai, China) provided Resiquimod (R848). Beyotime Biotechnology sold a Calcein/PI Cell Double Staining kit. Mouse tumor necrosis factor a (TNF-a), mouse interleukin 2 (IL-2) and mouse interferon gamma (IFN-γ) ELISA kits were purchased from BYabscience (Nanjing, China). We bought recombinant murine IL-4 from Peprotech. Sigma-Aldrich (St. Louis, USA) provided the fetal bovine serum (FBS), Hank's balanced salt solution (10HBSS), Dulbecco's phosphate buffer saline (DPBS), streptomycin (100 mg/mL), penicillin (100 IU/mL), and trypsin (2.5%).

2.2 Preparation of ICG@C3F8-R848 NBs. We have prepared ICG@C3F8-R848 NBs utilizing the thin-film hydration ultrasonic technique, as reported in earlier publications.[32] First, combine DSPC and DSPE-PEG-2000 in a 9:1 mass ratio. Then, add 10 ul of 5 mM R848 in a 2:1 vol/vol solution of methylene chloride and methanol. Transfer the aforementioned solution to a beaker and allow it to evaporate to create a lipid film after fully combining and dissolving it. A lipid suspension of the dried film was created using 5 mL of 100 ug/mL ICG in PBS. The suspension was then 20 times extruded using a micro-extruder (Avanti Polar Lipids, Alabaster, AL) through a 200 nm membrane. After that, the syringe was drained and filled with pure air before the squeezed suspension was transferred to a sealed vial. The mixture was then resuspended in 2 mL of PBS solution and physically agitated for 60 seconds in a dental mixer (made by YJT Medical Apparatus and Instruments, Shanghai, China) before being stored at 4 °C. Every procedure is completed in a dim setting. The same procedure can be used to create nanobubbles without R848.

Characterization

The dynamic light scattering (DLS, Malvern, UK) method was used to determine the nanomedicine's particle size and PDI value. By observing the size and PDI changes over a short period of time, the stability of nanomedicine was assessed. Transmission electron microscopy (TEM, JEOL, Japan) was used to examine the morphology of nanoparticles. The absorption spectra of R848, ICG, and ICG@C3F8-R848 NBs were recorded by using UV–vis spectrometer (SHIMADZU, Japan). ICG@C3F8-R848 NBs' sonodynamic properties were evaluated by measuring the amount of singlet oxygen ($_1O^2$) produced using a fluorescence spectrometer. As a probe for $_1O^2$, singlet oxygen sensor green (SOSG) was employed. The SOSG's fluorescence changes were monitored at the appointed time, with or without ultrasound.

Cell Culture

Murine hepatocellular carcinoma cell line-derived Hepa 1–6 cells were purchased from Procell Life Technologies Co., Ltd. (Wu Han, China), and grown in DMEM media with 10% FBS at 37 °C and 5% CO_2 in a humid incubator.

Intracellular ROS Detection

In brief, Hepa 1–6 cells were incubated with R848, ICG@C3F8-R848 NBs, ICG@C3F8 NBs+SDT, or ICG@C3F8-R848 NBs+SDT for 4h at the equivalent doses of ICG and R848. Afterward, Hepa 1–6 cells were treated with DCFH-DA for 20 min. And the other cells were cultured in the dark and were rinsed twice with DMEM, the cells in the SDT groups were exposed to ultrasound for 30s (1.0 W/cm^2) before being swiftly examined under a fluorescent microscope.

Cell Viability of Hepa 1–6 Cells

Hepa 1–6 cells were seeded at a density of 1×10^4 cells per well in 96-well plates and cultivated for 24 hours. After the treated with different ICG concentrations (0, 40, 80, 100, 150, 200, 250, 300, 600 μg/mL) of ICG@C3F8-R848 NBs and ICG@C3F8 NBs, they were exposed to LFUS for 30s (1.0 W/cm^2) 24 h later, all of the cells were assessed by CCK8 assay for another 4 h.

Measuring the Potential of the Mitochondrial Membrane

A JC-1 (Beyotime, C2005) detection kit was used to find the potential of the mitochondria. Hepa 1–6 cells were treated in the four treatment groups (PBS, R848, ICG@C3F8-R848 NBs, ICG@C3F8 NBs+SDT, and ICG@C3F8-R848 NBs +SDT) and then stained with JC-1 for 20 minutes before being twice washed with buffer solution. The labeled cells were examined under a fluorescence microscope after being added ice PBS solution.

Cell Apoptosis Testing and Live/Dead Cell Labeling

Hepa 1–6 cells were treated with PBS, R848, ICG@C3F8-R848 NBs, ICG@C3F8 NBs+SDT, and ICG@C3F8-R848 NBs+SDT at the equivalent quantities of ICG and R848, for the live/dead cell staining experiment. The SDT groups' cells were then exposed to ultrasound for 30s while the control groups were not. The cells were stained with Calcein-AM /PI for 20 minutes after twenty-four hours. A fluorescence microscope observed the cellular fluorescence.

Hepa 1–6 cells were subjected to the aforementioned groups' respective treatments for the cell apoptosis assay. The cells were then gathered and stained for 20 minutes using Annexin V-FITC/PI. Hepa 1–6 cells were cleaned with PBS before being subjected to a flow cytometry examination to identify cell apoptosis.

Isolation of Murine BMDMs and Macrophage Repolarization into an M1-Like Phenotype in vitro

Femur and tibia bones from male 6–8-week C57BL/6 mice were removed, and then they were further sliced and flushed with cold PBS (pH 7.4), aided by a needle, to a Petri dish in order to isolate murine bone marrow-derived macrophages (BMDMs). The cell solution was then diluted with 1.2 mL of PBS (pH 7.4) before being centrifuged at 500 g for 5 min. after that, the red blood cells were removed and the suspension was resuspended with 400 uL RBC lysate for 2 min. The

BMDMs were plated in 6-well plates at 37°C after being suspended in RPMI with 25ng/mL of the macrophage colony-stimulating factor (M-CSF, novoprotein, China). 1 mL of fresh RPMI containing 25 ng/mL of M-CSF was substituted for 1 mL of the cell culture medium after 3 days. RPMI non-tissue culture supplemented with 20 ng/mL of interleukin (IL)-4 (ProteinTech, China) was used to treat resting macrophages (M0 macrophages) after 6 days in order to differentiate them into M2-like macrophages, which were then cultured for 48 hours at 37 °C before being characterized. Cells were washed three times with PBS, then cultured for 24 hours with several groups (PBS, R848, ICG@C3F8 NBs, ICG@C3F8 NBs +SDT, and ICG@C3F8-R848 NBs+SDT) to test the capacity of NPs to repolarize M2-like macrophages into M1-like phenotype. After that, cells were labeled with Biolegend antibodies against PE-F4/80, PE/Cy7-CD86, and BV421-CD206 before being examined by flow cytometry (BD Biosciences LSRFortessa X-20). However, qRT-PCR was used to analyze the expression of the M1 marker (CD86, TNF-α, IL-6) and the M2 marker (Arg-1, CD206, CD163) in M2 macrophages following therapy. Each group's three samples were examined.

In vivo Tumor Model

The male C57BL/6 mice were obtained from the Laboratory Animal Center of Southern Medical University, and used at the age of 6 weeks. The tumor-bearing mice were prepared by subcutaneous injection at the right back of cell suspension containing 5×10^6 Hepa1–6 cells (mouse liver cancer cells). This study was approved by the Ethics Committee for Animal Experiments of Harbin Medical University. All animal experimental procedures (including the mice euthanasia procedure) were conducted according to the Association for Assessment and Accreditation of Laboratory Animal Care and the Institutional Animal Care and Use Committee guidelines.

Biodistribution and in vivo and ex vivo Imaging

For in vivo imaging, Then Hepa 1–6 tumor-bearing C57BL/6 mice were injected intravenously with 200 μL free ICG and ICG@C3F8-R848 NBs in PBS, respectively, with the same concentration of ICG. All mice were gaseously sedated at various time intervals (1, 4, 8, 12, 24, and 48 h) following injection, and in vivo fluorescence imaging was captured by a small animal imaging system (excitation/emission=605/690 nm). Then, all mice were sacrificed at different time points, and their tumors, hearts, liver, spleens, lungs, and kidneys were collected for ex vivo signals acquiring. Furthermore, the tumor was prepared in a frozen section through the longitudinal cutting sectioned longitudinally. A fluorescence microscope was used to observe the tumor's sample distribution.

Antitumor Effect in vivo

To perform the in vivo tumor therapy, the C57BL/6 mice with subcutaneous Hepa1–6 xenografts (grew up to approximately 150–200 mm^3) were divided into five groups according to the different treatments. (n=10 per group): Group A: PBS, Group B: ICG@C3F8-R848 NBs, Group C: R848, Group D: ICG@C3F8 NBs+SDT, Group E: ICG@C3F8-R848 NBs+SDT. The mice were irradiated with ultrasound for 2 min (1 W/cm^2) after injecting intravenously for 24h. Every two days, the mice's body weight and tumor volume were recorded. The formula tumor volume=length1/2width^2 was used to get the tumor volume. On day 17, mice were put to death, and blood and tumors were collected for additional research. Each group (n=3) had its blood drawn, and it was centrifuged for 20 minutes at 4 °C and 2000 g. Aspartate aminotransferase (AST), alanine aminotransferase (ALT), Glutamyl transpeptidase (GGT), total bilirubin (TBIL), blood urea nitrogen (UREA), and creatinine (CRE) were among the liver and renal functions assessed using plasma samples by Pointcare M3 (MNCHIP, China). The removed tumors were embedded in paraffin, fixed with 4% paraformaldehyde, and cut into 10 μm pieces. TUNEL and immunofluorescence labeling for CD80 (TAMs that resemble M1 TAMs) and CD206 (TAMs that resemble M2 TAMs) were used to mark tumor sections. On day 17, the mice's major organs were also stained with H&E and examined.

Flow Cytometry Analyses of Intra Tumoral TME Cells

After immunofluorescence staining, tumor-infiltrating lymphocytes from tumor tissues (n=3) were separated into single-cell suspensions, and their quantitative analysis by flow cytometry was performed. In a nutshell, tumor tissues were removed from dead mice, cut into small pieces with a razor, and then digested enzymatically at 37°C for 60 minutes with collagenase IV and DNase. The BD Biosciences LSRFortessa X-20 FACS system was used to collect the cells, stain them

using a combination of fluorescence-conjugated antibodies, and analyze the results. The following monoclonal anti-mouse antibodies were used: PE-F4/80(Biolegend), PE/Cy7-CD80(Biolegend), BV421-CD206(Biolegend), FITC-CD45 (Tombo), PE/Cy5.5-CD3 (Biolegend), APC-CD4(Biolegend), PE-CD8a(Biolegend), BV421-CD25(Biolegend), PE-FOXP3 (eBioscience), BV510-CD11b(Biolegend), APC-Gr-1(Biolegend), and PE- F4/80(Biolegend).

Statistical Analysis

There were three duplicates of each experiment. The biological statistics are computed as the standard deviation of the average of three replicates and are shown as percentages. All sample values were compared using GraphPad Prism 8.0's Student's *t*-test with the control (untreated cells) value, which was taken as 100% of all sample values. P values of 0.05, 0.01 and 0.001 were used to determine if the control and sample values were significant, highly significant, or extremely significant.

Results

ICG@C3F8-R848 NB Preparation and Characterization

ICG@C3F8-R848 NBs were synthesized using the self-assembly method, as depicted in Figure 1A, with the sonosensitizer ICG and R848 serving as the building blocks. Transmission Electron Microscope (TEM) images of ICG@C3F8-R848 NBs, presented in Figure 1B and Figure S1, displayed a uniform nanospheres morphology with an average

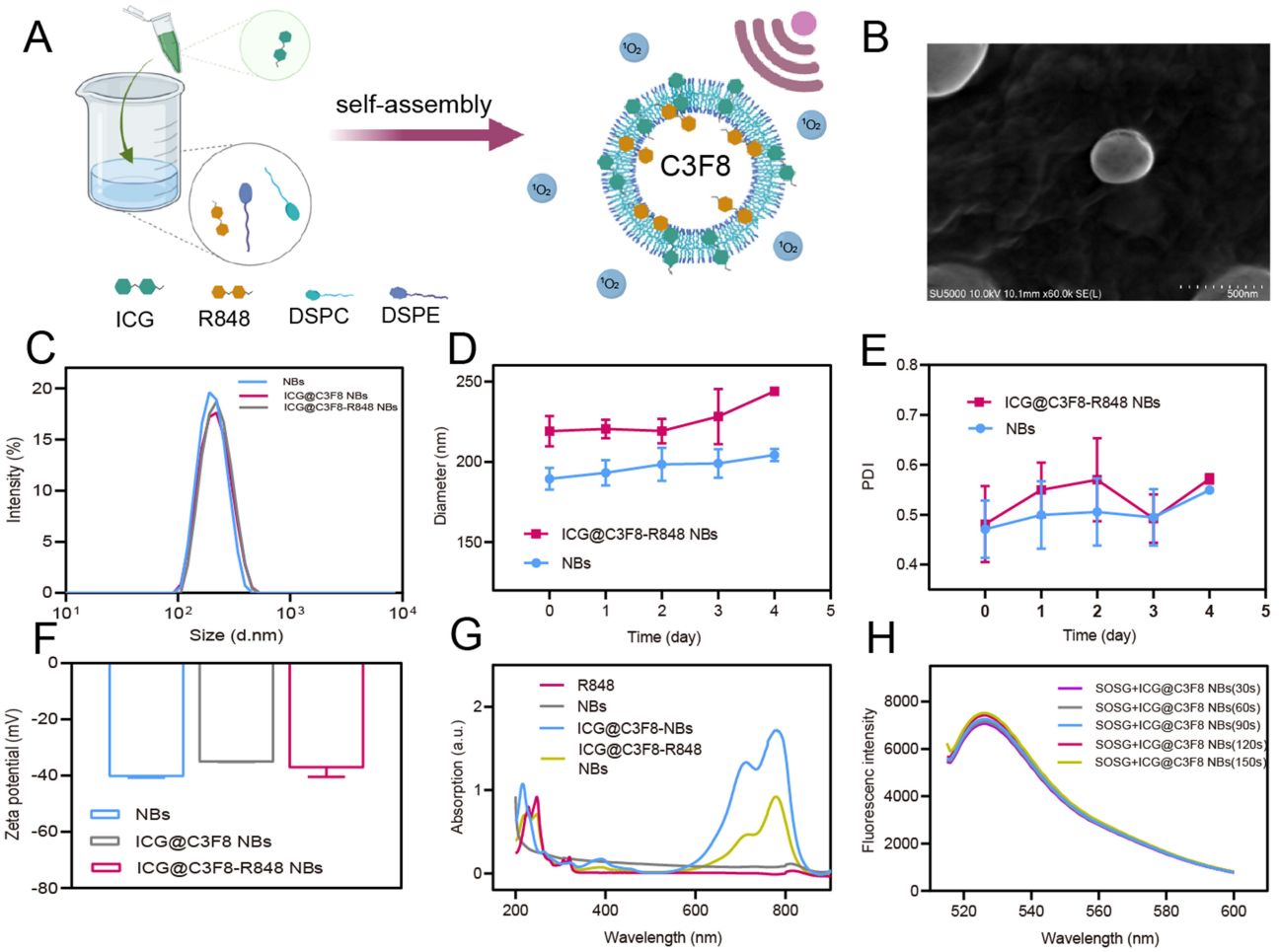

Figure 1 Preparation and characterization of ICG@C3F8-R848 NBs. (**A**) ICG@C3F8-R848 NBs were prepared based on the sonosensitizer of ICG and the TLR agonist of R848 through intermolecular interactions. (**B**) Transmission electron microscopy image showing a quasi-spherical morphology of ICG@C3F8-R848 NBs with a mean diameter of about 220 nm, Scale bar = 500 nm; (**C**) The DLS results showed a mean particle size of ICG@C3F8-R848 NBs to be 219.2±7.7 nm. (**D**) Size stability of the free NBs and ICG@C3F8-R848 NBs over 4 days. (**E**) Polydispersity value stability of free NBs and ICG@C3F8-R848 NBs over 4 days. (**F**) The Zeta potential of ICG@C3F8-R848 NBs to be −37.3±3.2 mV; (**G**) UV-vis spectra of ICG, NBs, ICG@C3F8 NBs and ICG@C3F8-R848 NBs. (**H**) Time-dependent SOSG absorption spectra in the presence of ICG@C3F8-R848 NBs under US irradiation for varied durations.

diameter of approximately 220 nm. This was further supported by dynamic light scattering (DLS) measurements, shown in Figure 1C, which revealed a mean diameter of ICG@C3F8-R848 NBs as 219.2±7.7 nm. Furthermore, continuous monitoring of size and polydispersity index (PDI) changes, depicted in Figure 1D and E, exhibited permissible variations. The zeta potential of the complex was concurrently measured as −37.3±2.2 mV (Figure 1F). The absorption spectrum of ICG@C3F8-R848 NBs, depicted in Figure 1G, displayed absorption peaks at approximately 780 nm and 240 nm. Moreover, Figure 1H demonstrated a positive correlation between the lengthening of the ultrasonic irradiation period and the fluorescence intensity of SOSG.

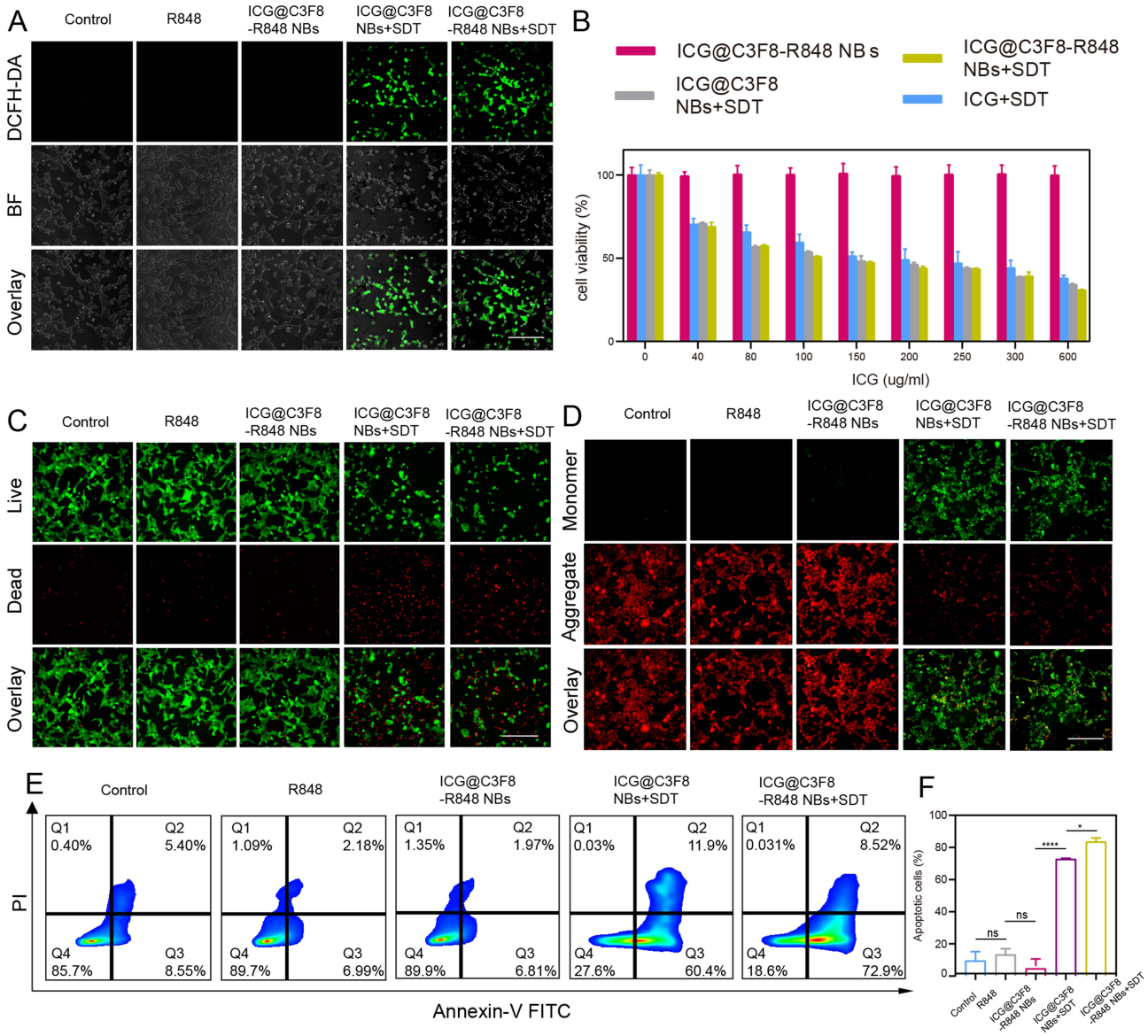

Figure 2 In vitro curative effect of the ICG@C3F8-R848 NBs upon SDT. (**A**) Fluorescence images analyses of intracellular ROS generation as indicated by DCFH-DA detection after receiving different treatments as indicated. (Scale bar = 50 μm). (**B**) Cytotoxicity analysis of differential treatments at different concentrations. (**C**) Representative fluorescence images of cells stained with calcein AM (green, live cells) and propidium iodide (red, dead cells) in different treatment (scale bar = 50 μm). (**D**) Fluorescence images of the JC-1 monomer (green channel), and aggregate (red channel) in the mitochondria of HCC cells after differential treatments as indicated. (scale bar = 50 μm). (**E**) The apoptotic frequency was analyzed by flow cytometry after different treatments. Total apoptosis rate was calculated by Q2 (early apoptosis) and Q3 (late apoptosis). (**F**) Quantification of the total apoptosis rates. Data are expressed as mean ± SD (n = 3). Statistical significances were calculated via one-way analysis of variance (ANOVA). *P < 0.05, ****P < 0.0001.

SDT Intracellular ROS Detection

Fluorescence microscope analysis was conducted to evaluate the intracellular ROS levels, as illustrated in Figure 2A. Hepa 1–6 cells treated with ICG@C3F8 NBs and ICG@C3F8-R848 NBs exhibited minimal fluorescence. However, upon ultrasound exposure, both ICG@C3F8 NBs and ICG@C3F8-R848 NBs induced noticeable green fluorescence in Hepa 1–6 cells. For the quantification of singlet oxygen ($_1O^2$) generation in aqueous solution, 1.3-diphenylisobenzofuran (DPBF) was used as an indicator. As shown in Figure S2, under the action of SDT, both ICG@C3F8 NBs and ICG@C3F8-R848 NBs have excellent ROS generation efficiency.

Cytotoxicity of Therapeutic Effect in vitro

Cytotoxicity assessments were performed on different nanoparticles (NPs) both with and without ultrasound (US) treatment. As depicted in Figure 2B, the viability of Hepa 1–6 cells was not significantly affected by US as the concentration of NPs increased. Additionally, at the same ultrasonic concentration, there was no discernible difference in cytotoxicity between ICG@C3F8 NBs and ICG@C3F8-R848 NBs.

Subsequently, live/dead and JC-1 cell staining tests were conducted. The presence of US, combined with ICG@C3F8 NBs and ICG@C3F8-R848 NBs, led to increased cell death due to the potent SDT efficacy, as illustrated in Figure 2C and D. Furthermore, cells treated with ICG@C3F8 NBs and ICG@C3F8-R848 NBs exhibited similar red and green fluorescence.

Moreover, flow cytometry was employed to examine cell apoptosis in greater detail, as shown in Figure 2E. ICG@C3F8 NBs, ICG@C3F8-R848 NBs, and R848 alone did not induce cell apoptosis in the absence of US. However, in the presence of US, SDT using ICG@C3F8 NBs and ICG@C3F8-R848 NBs resulted in 72.3% and 81.4% of tumor cells undergoing apoptosis respectively (Figure 2F).

In addition, we used immunofluorescence to detect the protein expression level of CRT in Hepa 1–6 cells to determine the efficiency of inducing ICD. The Hepa 1–6 cells used in this study were purchased from Procell Life Technologies Co., Ltd. (Wu Han, China). Compared with the Control group and ICG@C3F8-R848 NBs, when ICG@C3F8-R848 NBs were combined with SDT, the expression of CRT protein increased significantly, indicating that it has the best ICD induction efficiency. (Figure S3).

In vitro Repolarization of Macrophages with M2-Like Phenotype into M1-Like Phenotype

Subsequently, we investigated the in vitro repolarization using primary mouse macrophages exhibiting characteristics of M2 cells. Flow cytometry analysis of macrophages treated with ICG@C3F8-R848 NBs+US revealed a higher CD86 to CD206 ratio compared to the R848 alone group, as depicted in Figure 3A and C. Furthermore, the mRNA levels of M1 markers were significantly higher in the ICG@C3F8-R848 NBs+US treatment group compared to the R848 alone groups, while the mRNA levels of M2 markers were lower, as shown in Figure 3D–I.

In vivo, Ex-Vivo Biodistribution Analysis and Antitumor Effect in vivo

In order to assess the biological distribution and tumor targeting capability of the composite nanobubbles, we examined the fluorescence distribution of ICG. When free ICG was injected, the fluorescence was mainly observed in metabolic organs such as the liver and spleen at different time points, with only a faint signal detected at the tumor location after 24 hours. However, when ICG@C3F8-R848 NBs were administered, the tumor exhibited the strongest fluorescence signal, as shown in Figure 4C and S4. Notably, the fluorescence signal in the tumor showed little decrease over time.

Furthermore, tumor sections were used to evaluate the distribution of ICG fluorescence, as depicted in Figure 4D. The fluorescence intensity of ICG@C3F8-R848 NBs was significantly higher compared to free ICG in the tumor interior, confirming the enhanced tumor targeting ability of the composite nanobubbles.

Figure 4A illustrates the in vivo cancer treatment regimen. The inhibitory effects of various therapeutic modalities on tumor growth were assessed based on differences in tumor sizes, as shown in Figure 4E. The ranking of the therapeutic modalities from least to most effective was as follows: PBS = ICG@C3F8-R848 NBs < ICG@C3F8 NBs +

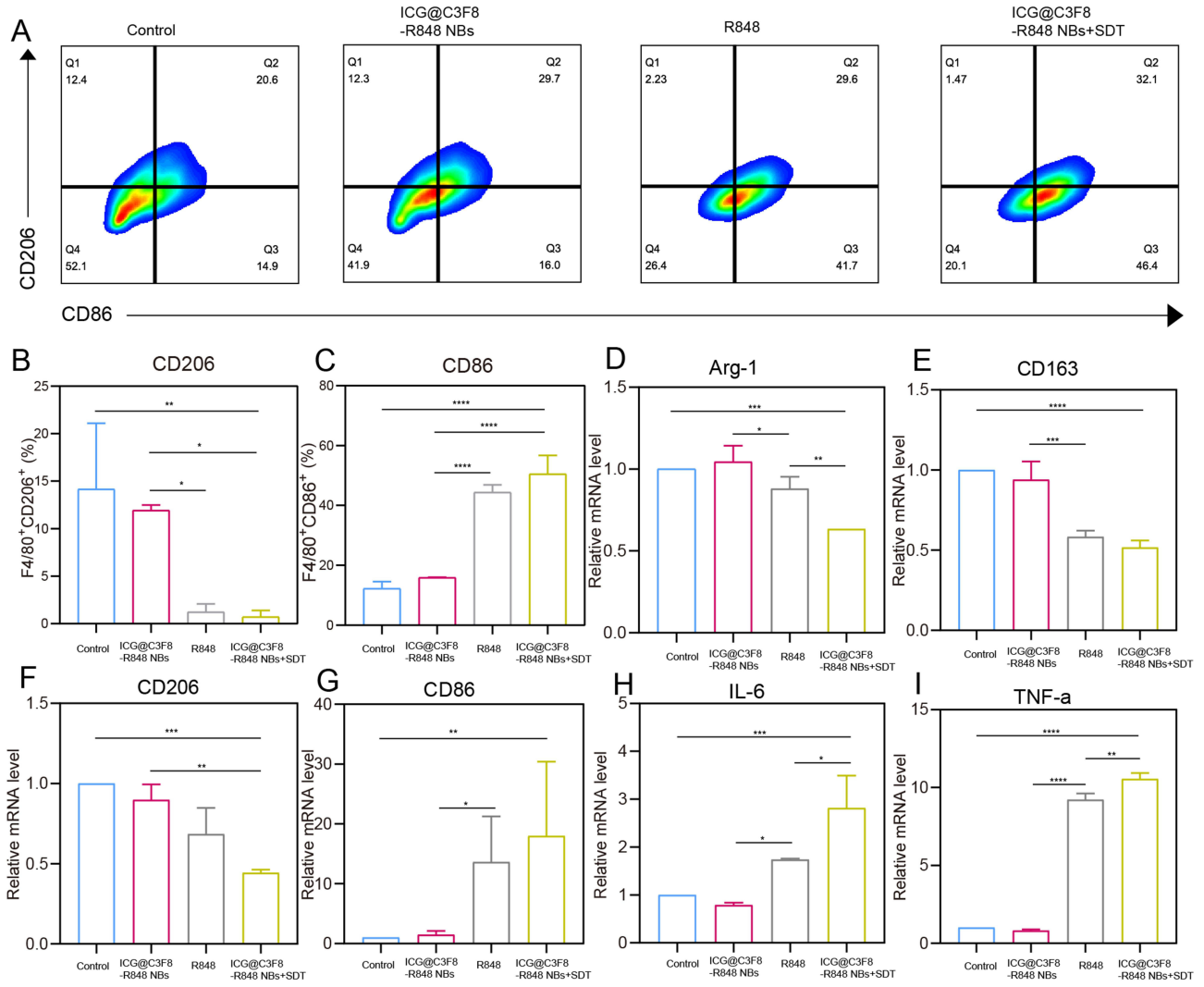

Figure 3 In vitro repolarization of M2 macrophages. (**A**) Flow cytometry and (**B** and **C**) quantitative analysis of M1 macrophages and M2 macrophages by CD86 marker and CD206 marker. (**D**–**I**) Relative expressions mRNA in M2 macrophages (Arg-1, CD163 and CD206) and M1 (CD86, IL-6 and TNF-α) as evaluated by qRT-PCR (n=3 biologically independent experiments). The data represent mean ± SD, one-way ANOVA, *P < 0.05, **P < 0.01, ***P < 0.001, ****P < 0.0001.

SDT < R848 < ICG@C3F8-R848 NBs + SDT. It was observed that ICG@C3F8 NBs + SDT and R848 therapy only marginally slowed tumor growth, while the ICG@C3F8-R848 NBs+SDT-treated group exhibited significantly stronger tumor-suppressing effects. This was further supported by hematoxylin and eosin (H&E) and terminal-deoxynucleotidyl transferase-mediated dUTP-biotin nick end labeling (TUNEL) staining, as shown in Figure 4G and H, which revealed more prominent necrotic and apoptotic cells in the ICG@C3F8-R848 NBs+SDT-treated group compared to the other groups.

Additionally, in vivo biosafety analysis was conducted to evaluate indicators such as body weight and biochemical blood indices, as biosafety is of utmost relevance to life and health. No discernible changes were observed in the aforementioned indicators in all treatment groups Figure 4F and Table S1. Similarly, the control group and the ICG@C3F8-R848 NBs-treated group, ICG@C3F8 NBs + SDT, R848, and ICG@C3F8-R848 NBs+SDT-treated group showed no discernible variations in the main blood chemistry parameters, including creatinine (CRE) and blood urea nitrogen (BUN) for the kidney, and alkaline phosphatase (AKP), aspartic acid transferase (AST), and alanine amino-transferase (ALT) for the liver, as depicted in Figure S5. Additionally, H&E staining revealed no signs of histological damage in the heart, liver, spleen, or kidney, as shown in Figure S7. These findings indicate that these treatment modalities exhibit good hemocompatibility and histocompatibility.

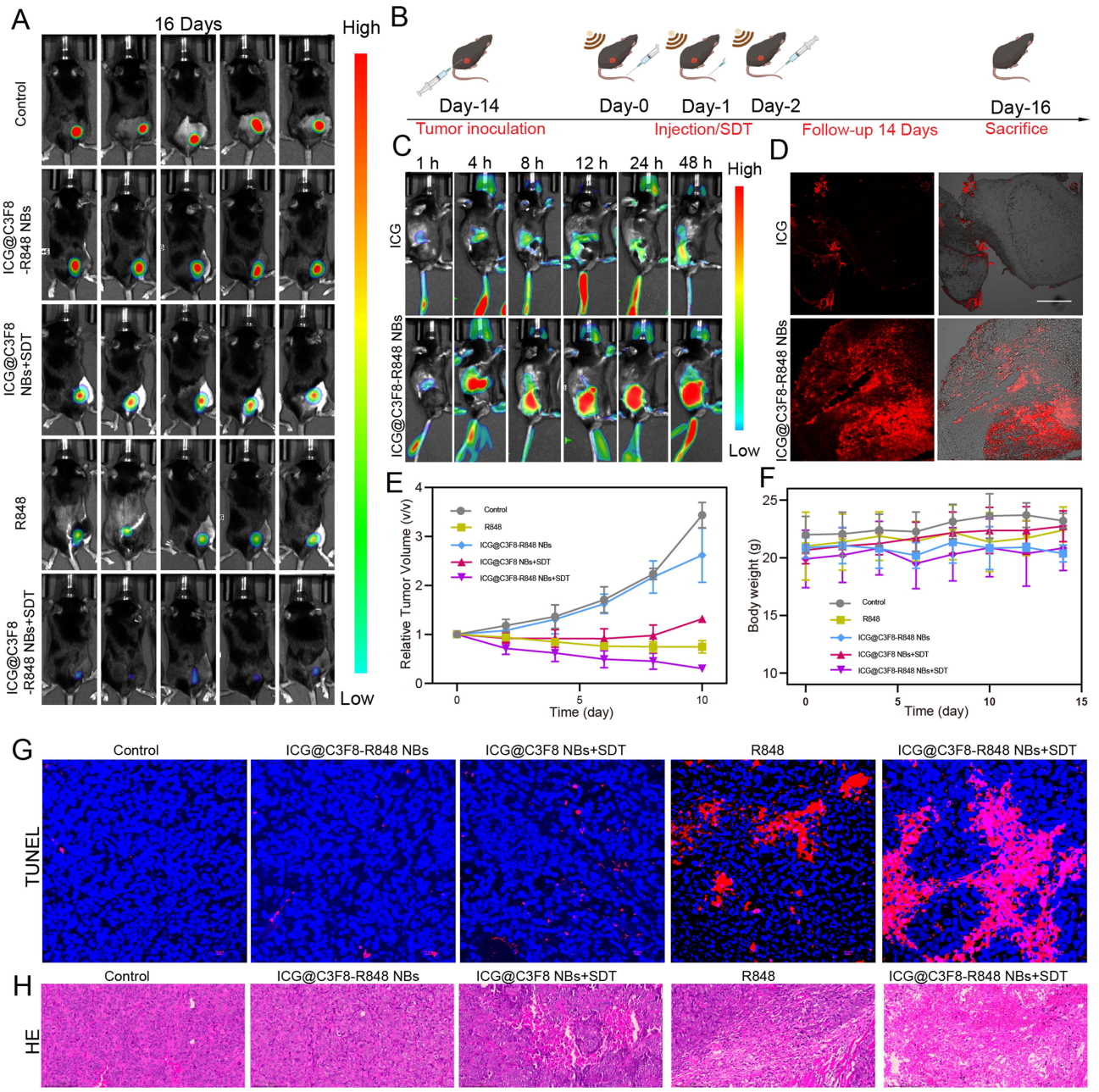

Figure 4 Experimental results of synergistic sono-immunotherapy in vivo. (**A**) Bioluminescence images of tumor-bearing mice in different groups at the 16 th days of the follow-up period. (**B**) Schematic illustration of synergistic sono-immunotherapy strategy against subcutaneous transplant tumor. (**C**) In vivo distribution of free ICG and ICG@C3F8-R848 NBs in tumor-bearing mice at different time points. (**D**) The fluorescence intensity of ICG@C3F8-R848 NBs and ICG alone in the tumor interior. Scale bar = 200 μm. (**E**) Tumour-growth curves of different groups of tumour-bearing mice after various treatments as indicated in the figure. (**F**) Weight of tumour-bearing mice of different groups after various treatments as indicated in the figure. (**G** and **H**) TUNEL and H&E staining for pathological changes in the tumor tissue. Scale bar = 10 μm. Scale bar = 100 μm.

In vivo Macrophage Polarization and Antitumor Immune Activation

In the study, Hepa 1–6 tumor-bearing mice were administered intravenous injections of therapeutic agents. Following this, the mice were euthanized, and an immunological analysis of the tumor tissues was conducted.

As depicted in Figure 5A, S8C and D, the group treated with ICG@C3F8-R848 NBs in combination with ultrasound (US) exhibited the greatest increase in tumor-infiltrating $CD4^+CD8^+$ T cells. This finding confirmed that ICG@C3F8-R848 NBs with US can effectively activate cytotoxic T lymphocytes (CTLs) for immunotherapy, as the frequency of $CD4^+CD8^+$ T cells in the ICG@C3F8-R848 NBs with US group was higher than that in the control group. It is worth

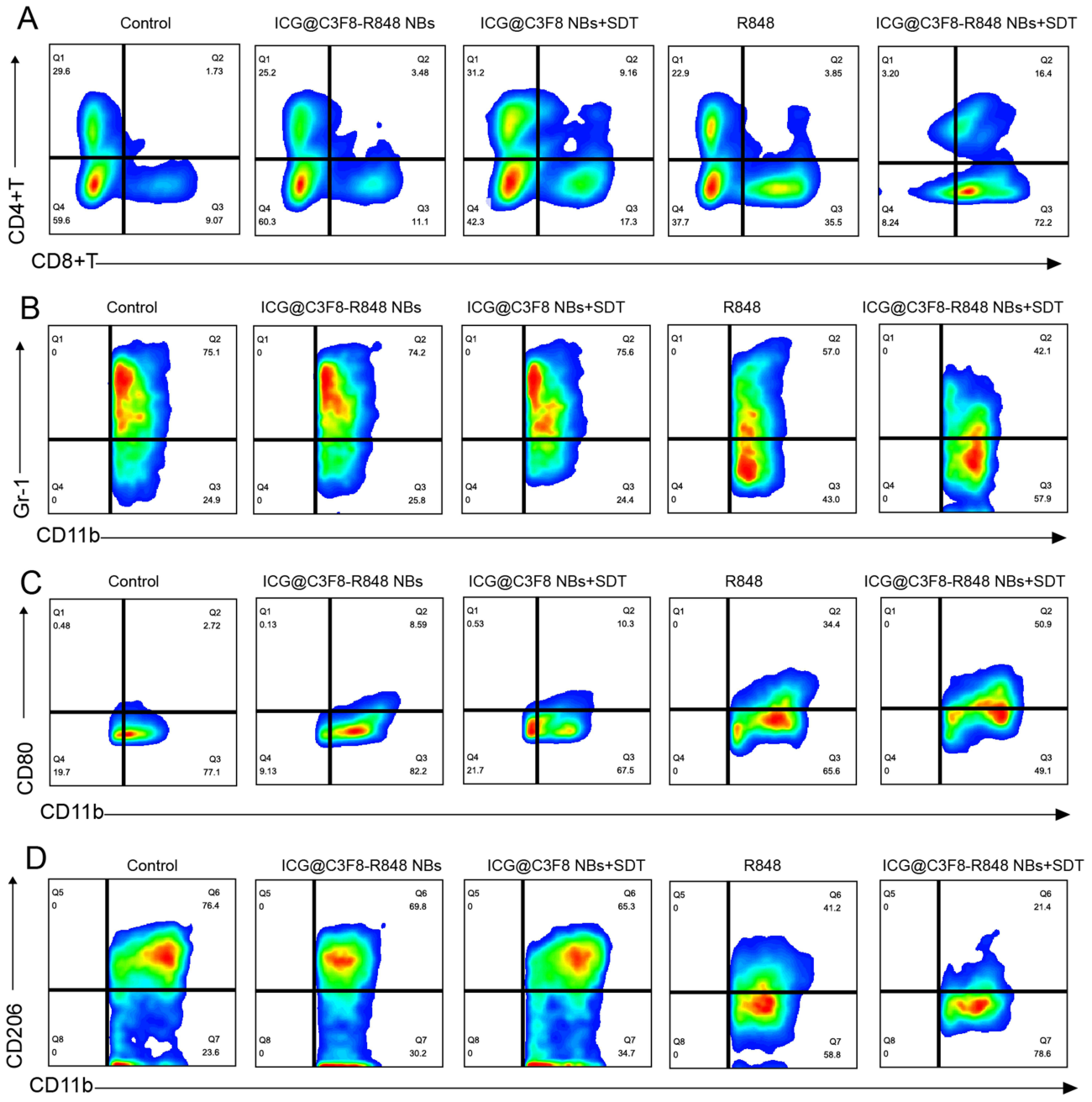

Figure 5 Analysis of immune cells in experimental animals after synergistic sono-immunotherapy. (**A**) Flow cytometry analysis of $CD4^+$ T cells and $CD8^+$ T cells. (**B**) Flow cytometry analysis of MDSCs by GR-1 marker. (**C** and **D**) Flow cytometry analysis of M1 macrophages and M2 macrophages by CD80 marker and CD206 marker.

noting that the proliferation and activation of CTLs may be hindered by myeloid-derived suppressor cells (MDSCs), leading to detrimental immunosuppression. However, when compared to the control group, the use of ICG@C3F8-R848 NBs with US resulted in a 50% reduction in MDSC differentiation (Figure 5B and S8E), indicating an enhanced immunosuppressive microenvironment in vivo.

Furthermore, flow cytometry analysis (Figure 5C, D, S8A and S8B) demonstrated that both R848 and ICG@C3F8-R848 NBs with US treatment led to an increase in the number of M1 macrophages and a decrease in the number of M2 macrophages, indicating enhanced macrophage polarization. The M1/M2 ratio of ICG@C3F8-R848 NBs with US treatment significantly increased compared to the control group, suggesting effective polarization of tumor tissues by macrophages for immunotherapy. Notably, the polarization effect induced by ICG@C3F8-R848 NBs in the presence of

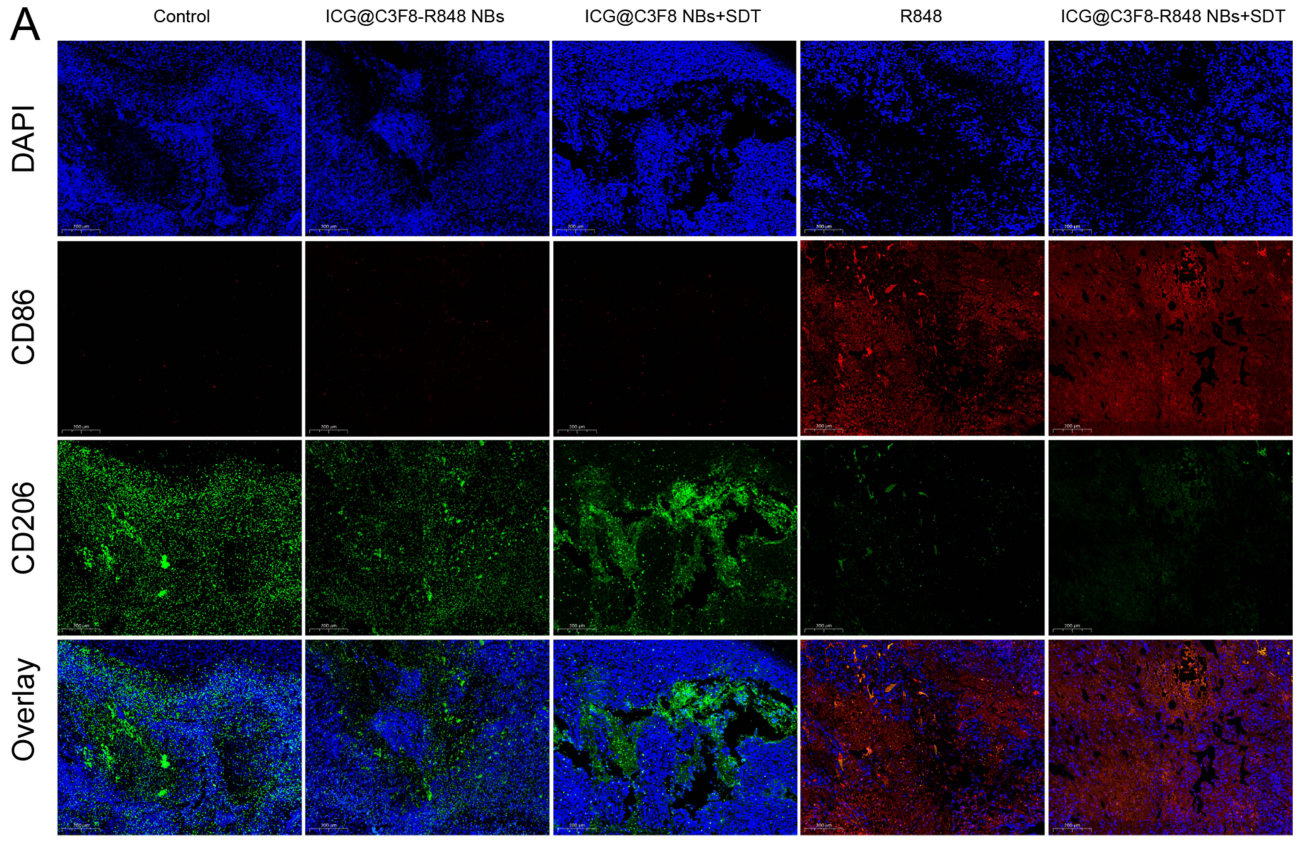

Figure 6 Analysis of immune cells in experimental animals after synergistic sono-immunotherapy. Representative immunofluorescence images of CD86 marker and CD206 marker expressions in the tumor tissues. Scale bars = 200 μm.

US irradiation did not show significant changes, indicating that the TLR agonist R848 primarily facilitated the polarization of tumor-associated macrophages. Immunofluorescence staining also revealed that tumor-associated macrophages (TAMs) predominantly exhibited the M2 phenotype in the negative control group (Figure 6, Group A, red fluorescence), with only a small population showing the M1 phenotype. However, after 16 days of synergistic photo-immunotherapy, compared to the negative control group, the TAMs population exhibited a noticeably higher number of M1 macrophages (Figure 6, Group F, green fluorescence). In addition, we also evaluate the cytokine profiles from the animals by RT-qPCR. The concentrations of interleukin-2 (IL-2) and tumor necrosis factor-α (TNF-α) were much higher in the Group F than in the Group A, but the opposite trend was found for IL-4 and IL-10. These data suggested that the synergistic Photo-immunotherapy both increased the frequency of positive immune responders and suppressed negative immune inhibitors, and thus established an inflamed tumor immunity niche and exerted an effective tumoricidal immune activity that inhibited HCC regrowth (Figure S6).

Discussion

Ultrasound nanobubbles can not only assist ultrasound imaging but also enhance tumor treatment through drug delivery functions.[33] Nanobubbles are ultrasonic-responsive compared to traditional nano delivery systems. After reaching the target organ or target tissue, through ultrasound irradiation of different intensities, the microbubbles shrink, oscillate, expand, and rupture, finally leading to drug release.[34] At the same time, the cavitation and sonoporation effects produced by ultrasound irradiation cause the tumor vascular cell membrane to small holes are formed to promote the drug to enter the target tumor tissue, greatly improving the efficacy.[35,36] Numerous non-invasive therapies, such as High-Intensity Focused Ultrasound (HIFU), Photodynamic Therapy (PDT), and Sonodynamic Therapy (SDT), have gained significant attention as potential solutions to address the limitations of conventional cancer treatment methods. SDT, in particular, has shown promising results in inducing cancer cell death and reducing tumor growth in various preclinical tumor

models, including breast cancer, brain glioma, and pancreatic cancer. The combination of ICG@C3F8-R848 NBs nano sonosensitizer and R848 aims to trigger sono-immunotherapy and induce apoptosis in cancer cells.

First, a new type of nanobubbles was developed as a delivery system for nano-sono-sensitizers (Figure 1A). The nanobubbles' small size (nanoscale diameter, Figure 1B) allowed them to serve as nuclei for the cavitation effect during SDT. Combining SDT with nanobubbles resulted in a remarkable apoptotic rate of 80% (Figure 2E), while ICG@C3F8-R848 NBs alone did not induce significant apoptosis without Low-Intensity Focused Ultrasound (LIFU) irradiation (Figure 2E). Live/dead and JC-1 cell staining tests were conducted to evaluate cell activity levels (Figure 2C and D).

Secondly, flow cytometry analysis of macrophages treated with ICG@C3F8-R848 NBs and ultrasound (US) demonstrated a higher CD86 to CD206 ratio compared to the R848 group (Figure 2G and H). The increased repolarization efficiency of ICG@C3F8-R848 NBs with US compared to R848 alone may be attributed to enhanced cellular uptake.

Thirdly, the distribution of ICG fluorescence in composite nanobubbles and the immune activation effects in vivo were examined. Over time, the fluorescence in the tumor area gradually increased (Figure 3B), indicating efficient tumor site enrichment due to the enhanced permeability and retention (EPR) effect of the composite nanobubbles. In contrast, free ICG fluorescence was primarily localized in metabolic organs such as the liver and spleen. Notably, the fluorescence signal in the tumor area decreased minimally, indicating sustained presence in the tumor region.

In Figure 5A, the group treated with ICG@C3F8-R848 NBs and US showed the highest increase in tumor-infiltrating $CD4^+$ and $CD8^+$ T cells. This confirmed that ICG@C3F8-R848 NBs with US can activate cytotoxic T lymphocytes (CTLs) for immunotherapy, as the frequency of $CD4^+$ and $CD8^+$ T cells. in the ICG@C3F8-R848 NBs with US group was higher than that in the control group. Furthermore, it was observed that ICG@C3F8-R848 NBs with US reduced MDSC differentiation by 50% compared to the control group (Figure 5B), indicating an enhancement in the in vivo immunosuppressive microenvironment. Additionally, the M1/M2 ratio of ICG@C3F8-R848 NBs with US treatment significantly increased compared to the control group, suggesting effective polarization of tumor tissues by macrophages for immunotherapy (Figure S8A and B). Importantly, no significant difference in the polarization effect was observed when ICG@C3F8 NBs were used in conjunction with US irradiation, indicating that R848 primarily induced the polarization of tumor-associated macrophages. These findings were consistent with immunofluorescence staining results.

Conclusion

In summary, the study successfully developed a macrophage re-educator for SDT-initiated immunotherapy by combining sonosensitizers and TLR agonists. The self-assembled nanobubbles, ICG@C3F8-R848 NBs, demonstrated favorable properties such as uniform size, good dispersibility, and efficient tumor accumulation. The hydrophobic interaction played a crucial role in the self-assembly process. These nanobubbles exhibited superior sonodynamic performance and enhanced tumor cell death through SDT, leading to a potent immunogenic cell death (ICD) response and activation of cytotoxic T lymphocytes (CTLs). Furthermore, the ICG@C3F8-R848 NBs promoted the repolarization of M2 macrophages into M1 macrophages, which contributed to the rewiring of the tumor microenvironment and enhancement of antitumor immunity. The presence of R848 in the nanobubbles played a key role in inducing macrophage polarization. In in vivo studies, the SDT-initiated immunotherapy using ICG@C3F8-R848 NBs demonstrated significant suppression of tumor growth compared to the combination of SDT and immunotherapy alone. Overall, this research provides valuable insights into the development of personalized nanomedicine for cancer treatment. The combination of sonosensitizers, TLR agonists, and SDT holds promise for enhancing the efficacy of cancer therapy and stimulating the immune system's response against tumors.

Abbreviations

TME, tumor microenvironment; ICD, immunogenic cell death; HCC, hepatocellular carcinoma; SDT, sonodynamic treatment; ICG, Indocyanine green; NBs, nanobubbles; UTND, ultrasound-targeted nanobubble destruction; LFUS, low-frequency ultrasound; US, ultrasound; ITM, immune tolerance mechanisms; TAMs, tumor-associated macrophages; TLRs, Toll-like receptors; ROS, reactive oxygen species; HIFU, High-Intensity Focused Ultrasound; PDT, Photodynamic Therapy.

Supporting Information

Supporting Information is available from the author.

Data Sharing Statement

The data that support the plots within these paper and other findings of this study are available from the corresponding authors upon reasonable request.

Author Contributions

All authors made a significant contribution to the work reported, whether that is in the conception, study design, execution, acquisition of data, analysis and interpretation, or in all these areas; took part in drafting, revising or critically reviewing the article; gave final approval of the version to be published; have agreed on the journal to which the article has been submitted; and agree to be accountable for all aspects of the work.

Funding

This research was supported by the National Natural Science Foundation of China (grant number 82171947, 82202163, and 82202165).

Disclosure

The authors report no conflicts of interest in this work.

References

1. Sharma P, Hu-Lieskovan S, Wargo JA, Ribas A. Primary, adaptive, and acquired resistance to cancer immunotherapy. *Cell*. 2017;168(4):707–723. doi:10.1016/j.cell.2017.01.017
2. Krysko DV, Garg AD, Kaczmarek A, et al. Immunogenic cell death and DAMPs in cancer therapy, nature reviews. *Cancer*. 2012;12(12):860–875. doi:10.1038/nrc3380
3. Galluzzi L, Buqué A, Kepp O, Zitvogel L, Kroemer G. Immunogenic cell death in cancer and infectious disease, nature reviews. *Immunology*. 2017;17(2):97–111. doi:10.1038/nri.2016.107
4. Huang P, Qian X, Chen Y, et al. Metalloporphyrin-encapsulated biodegradable nanosystems for highly efficient magnetic resonance imaging-guided sonodynamic cancer therapy. *J Am Chem Soc*. 2017;139(3):1275–1284. doi:10.1021/jacs.6b11846
5. Yue W, Chen L, Yu L, et al. Checkpoint blockade and nanosonosensitizer-augmented noninvasive sonodynamic therapy combination reduces tumour growth and metastases in mice. *Nat Commun*. 2019;10(1):2025. doi:10.1038/s41467-019-09760-3
6. Chen J, Luo H, Liu Y, et al. Oxygen-self-produced nanoplatform for relieving hypoxia and breaking resistance to sonodynamic treatment of pancreatic cancer. *ACS Nano*. 2017;11(12):12849–12862. doi:10.1021/acsnano.7b08225
7. Zhang Q, Bao C, Cai X, et al. Sonodynamic therapy-assisted immunotherapy: a novel modality for cancer treatment. *Cancer Sci*. 2018;109(5):1330–1345. doi:10.1111/cas.13578
8. Song W, Kuang J, Li CX, et al. Enhanced immunotherapy based on photodynamic therapy for both primary and lung metastasis tumor eradication. *ACS Nano*. 2018;12(2):1978–1989. doi:10.1021/acsnano.7b09112
9. Zhang J, Chen C, Li A, et al. Immunostimulant hydrogel for the inhibition of malignant glioma relapse post-resection. *Nat Nanotechnol*. 2021;16(5):538–548. doi:10.1038/s41565-020-00843-7
10. Song C, Phuengkham H, Kim YS, et al. Syringeable immunotherapeutic nanogel reshapes tumor microenvironment and prevents tumor metastasis and recurrence. *Nature Commun*. 2019;10(1):3745. doi:10.1038/s41467-019-11730-8
11. Meurette O, Mehlen P. Notch Signaling in the Tumor Microenvironment. *Cancer Cell*. 2018;34(4):536–548. doi:10.1016/j.ccell.2018.07.009
12. Zou MZ, Liu WL, Gao F, et al. Artificial natural killer cells for specific tumor inhibition and renegade macrophage re-education. *Adv mater*. 2019;31(43):e1904495.
13. Zhai K, Huang Z, Huang Q, et al. Pharmacological inhibition of BACE1 suppresses glioblastoma growth by stimulating macrophage phagocytosis of tumor cells. *Nature Cancer*. 2021;2(11):1136–1151. doi:10.1038/s43018-021-00267-9
14. Lambrechts D, Wauters E, Boeckx B, et al. Phenotype molding of stromal cells in the lung tumor microenvironment. *Nat Med*. 2018;24(8):1277–1289. doi:10.1038/s41591-018-0096-5
15. Klichinsky M, Ruella M, Shestova O, et al. Human chimeric antigen receptor macrophages for cancer immunotherapy. *Nat Biotechnol*. 2020;38(8):947–953. doi:10.1038/s41587-020-0462-y
16. DeNardo DG, Ruffell B. Macrophages as regulators of tumour immunity and immunotherapy. *Nat Rev Immunol*. 2019;19(6):369–382. doi:10.1038/s41577-019-0127-6
17. Rodell CB, Arlauckas SP, Cuccarese MF, et al. TLR7/8-agonist-loaded nanoparticles promote the polarization of tumour-associated macrophages to enhance cancer immunotherapy. *Nat Biomed Eng*. 2018;2(8):578–588. doi:10.1038/s41551-018-0236-8
18. Wang YC, Wang X, Yu J, et al. Targeting monoamine oxidase A-regulated tumor-associated macrophage polarization for cancer immunotherapy. *Nat Commun*. 2021;12(1):3530. doi:10.1038/s41467-021-23164-2

19. Anderson NR, Minutolo NG, Gill S, Klichinsky M. Macrophage-based approaches for cancer immunotherapy. *Cancer Res*. 2021;81(5):1201–1208. doi:10.1158/0008-5472.CAN-20-2990
20. Feng Y, Mu R, Wang Z, et al. A toll-like receptor agonist mimicking microbial signal to generate tumor-suppressive macrophages. *Nature Commun*. 2019;10(1):2272. doi:10.1038/s41467-019-10354-2
21. Bahmani B, Gong H, Luk BT, et al. Intratumoral immunotherapy using platelet-cloaked nanoparticles enhances antitumor immunity in solid tumors. *Nat Commun*. 2021;12(1):1999. doi:10.1038/s41467-021-22311-z
22. Wagner J, Gößl D, Ustyanovska N, et al. Mesoporous silica nanoparticles as ph-responsive carrier for the immune-activating drug resiquimod enhance the local immune response in mice. *ACS Nano*. 2021;15(3):4450–4466. doi:10.1021/acsnano.0c08384
23. Islam MA, Rice J, Reesor E, et al. Adjuvant-pulsed mRNA vaccine nanoparticle for immunoprophylactic and therapeutic tumor suppression in mice. *Biomaterials*. 2021;266:120431. doi:10.1016/j.biomaterials.2020.120431
24. Ji G, Zhang Y, Si X, et al. Biopolymer immune implants' sequential activation of innate and adaptive immunity for colorectal cancer postoperative immunotherapy. *Adv Mater*. 2021;33(3):e2004559.
25. Liang JL, Luo GF, Chen WH, Zhang XZ. Recent advances in engineered materials for immunotherapy-involved combination cancer therapy. *Adv Mater*. 2021;33(31):e2007630.
26. Xu J, Xu L, Wang C, et al. Near-infrared-triggered photodynamic therapy with multitasking upconversion nanoparticles in combination with checkpoint blockade for immunotherapy of colorectal cancer. *ACS nano*. 2017;11(5):4463–4474. doi:10.1021/acsnano.7b00715
27. Wang L, Wang X, Yang F, et al. Systemic antiviral immunization by virus-mimicking nanoparticles-decorated erythrocytes. *Nano Today*. 2021;40:101280. doi:10.1016/j.nantod.2021.101280
28. Ryu KA, Stutts L, Tom JK, Mancini RJ, Esser-Kahn AP. Stimulation of innate immune cells by light-activated TLR7/8 agonists. *J Am Chem Soc*. 2014;136(31):10823–10825. doi:10.1021/ja412314j
29. Chen Y, Shang H, Wang C, et al. RNA-seq explores the mechanism of oxygen-boosted sonodynamic therapy based on all-in-one nanobubbles to enhance ferroptosis for the treatment of HCC. *Int J Nanomed*. 2022;17:105–123. doi:10.2147/IJN.S343361
30. Gao J, Liu J, Meng Z, et al. Ultrasound-assisted C(3)F(8)-filled PLGA nanobubbles for enhanced FGF21 delivery and improved prophylactic treatment of diabetic cardiomyopathy. *Acta Biomater*. 2021;130:395–408. doi:10.1016/j.actbio.2021.06.015
31. Du J, Li XY, Hu H, Xu L, Yang SP, Li FH. Preparation and imaging investigation of dual-targeted C(3)F(8)-filled PLGA nanobubbles as a novel ultrasound contrast agent for breast cancer. *Sci Rep*. 2018;8(1):3887. doi:10.1038/s41598-018-21502-x
32. Wu B, Yuan Y, Liu J, et al. Single-cell RNA sequencing reveals the mechanism of sonodynamic therapy combined with a RAS inhibitor in the setting of hepatocellular carcinoma. *J Nanobiotechnol*. 2021;19(1):177. doi:10.1186/s12951-021-00923-3
33. Yin T, Wang P, Zheng R, et al. Nanobubbles for enhanced ultrasound imaging of tumors. *Int J Nanomedicine*. 2012;7:895–904. doi:10.2147/IJN.S28830
34. Zhang C, Li Y, Ma X, et al. Functional micro/nanobubbles for ultrasound medicine and visualizable guidance. *Sci China Chem*. 2021;64(6):899–914. doi:10.1007/s11426-020-9945-4
35. Wang Y, Li X, Zhou Y, Huang P, Xu Y. Preparation of nanobubbles for ultrasound imaging and intracelluar drug delivery. *Int J Pharm*. 2010;384(1–2):148–153. doi:10.1016/j.ijpharm.2009.09.027
36. Bu X, Alheshibri M. The effect of ultrasound on bulk and surface nanobubbles: a review of the current status. *Ultrason Sonochem*. 2021;76:105629. doi:10.1016/j.ultsonch.2021.105629